Songklanakarin J. Sci. Technol.
32 (2), 197-200, Mar. - Apr. 2010

Songklanakarin Journal of Science and Technology
http://www.sjst.psu.ac.th

Original Article

Simulation of deformation fields underneath Vickers indenter: Effects of power-law plasticity

Nuwong Chollacoop[1]* and Upadrasta Ramamurty[2]

[1] *National Metals and Materials Technology Center (MTEC)*
Thailand Science Park, Klong Luang, Pathum Thani, 12120 Thailand.

[2] *Department of Metallurgy, Indian Institute of Science,*
Bangalore- 560012, INDIA

Received 28 September 2007; Accepted 20 March 2009

Abstract

The effects of power-law plasticity (yield strength and strain hardening exponent) on the plastic strain distribution underneath a Vickers indenter was systematically investigated by recourse to finite element simulation, motivated by the experimental macro- and micro-indentation on heat-treated Al-Zn-Mg alloy. For meaningful comparison between simulated and experimental results, the experimental heat treatment was carefully designed such that Al alloy achieve similar yield strength with different strain hardening exponent, and vice versa. On the other hand, full 3D simulation of Vickers indentation was conducted to capture subsurface strain distribution. Subtle differences and similarities were discussed based on the strain field shape, size and magnitude for the isolated effect of yield strength and strain hardening exponent.

Keywords: finite element, Vickers indentation, deformation field, power-law

1. Introduction

Instrumented sharp indentation, where load P and depth of penetration h being measured continuously, has been used widely as a non-destructive tool to probe and determine mechanical properties of the indented sample, due to its ease of sample preparation, requirement of small volume, and simple test procedure (Tabor, 1951; Doener *et al.*, 1986; Oliver *et al.*, 1992; Dao *et al.*, 2001). It is not surprising to see instrumented indentation being used to measure properties of materials at nano-, micro- and macro-scale, or in various disciplines ranging from biology, over food science, to pharmaceutical industry (Gouldstone *et al.*, 2007). Nonetheless, complex elastic-plastic contact mechanics during the indentation has called for direct experimental observation and computational comparison to support the limited theoretical framework. In a previous study (Srikant *et al.*, 2006) the cross-section deformation behavior underneath the Vickers indenter was experimentally investigated, following the method of Chaudhri (1998). The subsurface plastic strain distribution was then correlated to yield strength (σ_y) and the strain hardening exponent (n), according to power-law plasticity

$$\sigma = K\varepsilon^n, \quad (1)$$

where ε is plastic strain and K is a constant. In the present study, these correlations were compared to the simulation results of the Vickers indentation.

2. Experimental Procedure

Some results from the previous study (Srikant *et al.*, 2006) were described here for comparison with the simulation

*Corresponding author.
Email address: nuwongc@mtec.or.th

Table 1. Relevant mechanical properties of the aged alloys.

Aging time, t_a (h)	Young's Modulus, E (GPa)	Poisson ratio, ν	Yield Stress, σ_y (MPa)	Strain-hardening exponent, n
6			348	0.070
36	70	0.3	445	0.066
94			344	0.110

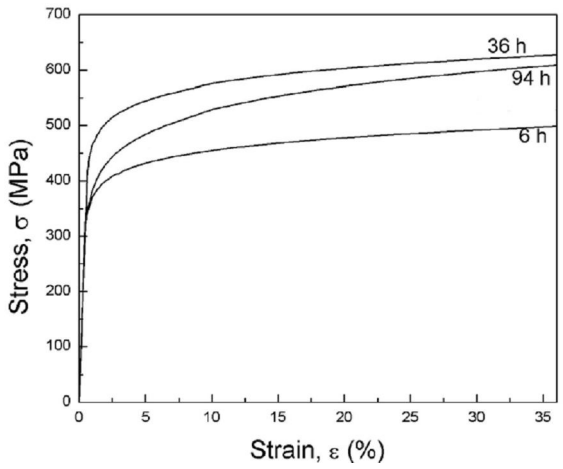

Figure 1. True stress-true strain curve for various aging samples.

findings. A commercial 7075 Al alloy (Al-7.6Zn-4.6Mg-1.0Si, wt%) was solutionized and properly aged to three conditions (6, 36, and 94 hrs) with elastic-plastic properties shown in Table 1 and Figure 1, according to power-law plasticity in Equation 1. Thus, two pairs of samples can be used to investigate the sole effect of yield strength (6 vs. 36 hrs) and strain hardening exponent (6 vs. 94 hrs). For each sample, macro-indentation with the Vickers tip using a load of 700 N was conducted with subsurface micro-indentation with the Vickers tip using a load of 0.5 N on the sectioned plane to provide plastic strain distribution map underneath macro-Vickers indentation, as shown in Figure 2. For experimental details, please refer to the previous study (Srikant *et al.*, 2006).

3. Computational Modeling

The simulation approached chosen for the present study was finite element analysis (FEA). Even though the macroscopic responses (*P-h* curve) of both Vickers and Berkovich indenters are similar to the cone with apex angle of 70.3° (Dao *et al.*, 2001, Chollacoop *et al.*, 2003), the microscopic detail of deformation field underneath the non-axis symmetric Vickers indenter requires a three dimensional computational model setup. Due to the symmetry of the Vickers indenter (pyramid with square base), only 1/8 of the full 3D-model was necessary, as shown in Figure 3.

The Vickers indenter was placed on top of the sample (plane *oab*) with loading direction along *oc* in the axis 3. Since the indentation depth is much smaller than the height of the unit cell (<1%) far-field conditions can be assumed in the numerical model. Hence, the bottom surface *cde* was simplified to be fixed in all directions; whereas the top plane *oab* and the outer plane *abd*e were free in all directions. The side plane *oaec* was allowed the displacements in axes 1 and 3 with rotation around axis 2; whereas the other side plane *obdc* was allowed the displacements in all axes 1, 2, and 3 under the constraint that plane *obdc* deformed in a planar fashion (displacements in axes 1 and 2 were identical). Finally, the centroid line can only move in axis 3. The contact

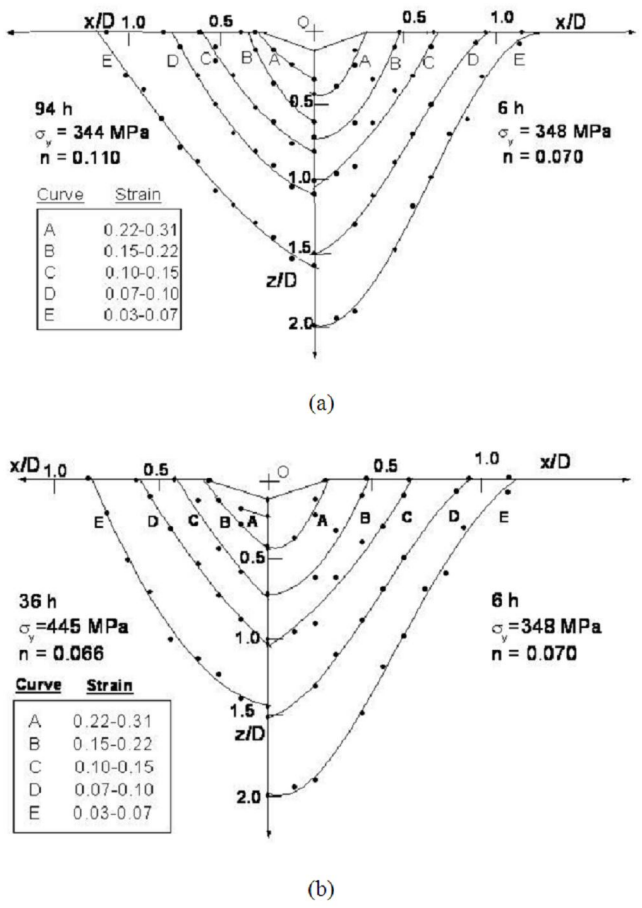

Figure 2. Experimental contour plot of plastic strain distribution underneath the Vickers indenter for (a) 6 vs. 94 hrs aged sample (similar σ_y but different n), and (b) 6 vs. 36 hrs aged sample (similar n but different σ_y). The contour line is drawn for visual help only.

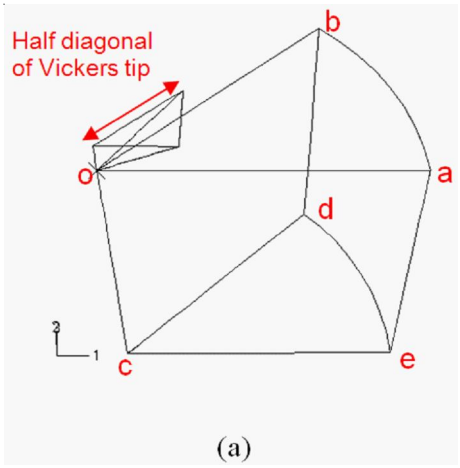

(a)

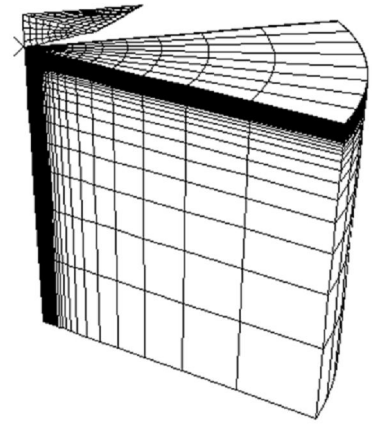

(b)

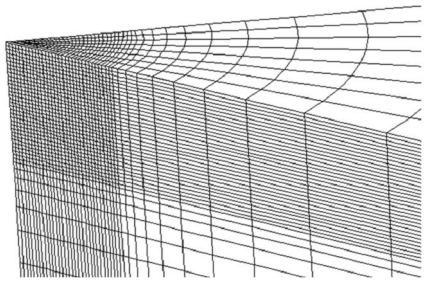

(c)

Figure 3. (a) Computational model setup for 3D Vickers indentation (only 1/8 is necessary due to its symmetry) showing (b) the overall mesh design, and (c) the mesh design at the contact region underneath the indenter (not shown here).

was defined between the rigid indenter bottom surface and the top plane *oab* with no friction since the effect of frictional contact is negligible (Bucaille *et al.*, 2003; Harsono *et al.*, 2008). The indented sample size was chosen to be much larger than the indentation depth during the simulated indentation. A fine mesh was designed for the contact region underneath the indenter tip to ensure enough contact elements, whereas a gradually coarser mesh was applied elsewhere (see Figure 3(b) and (c)). Thus, the model used the total of 17,224 8-node elements. The constitutive relation for each case was taken from the experimental curves in Figure 1.

4. Results and Discussion

Since the experimental macro-indentation was conducted at 700 N for all cases, the computational model was load-controlled. A slight difference was found if the contour plots were taken from the depth-controlled indentation simulation. After complete unloading, the contour plot of equivalent plastic strain (PEEQ) on the sectioned plane *oaec* was extracted from each case. Following Figure 2, the simulated contour plots are shown in Figure 4. Note that the contour line in Figure 2 was drawn for visual help only since it was more difficult to sharply define contour lines for the experimental results than for the computational results shown in Figure 4. Hence, each experimental contour line in Figure 2 spans a small range of plastic strain within a typical experimental scattering. On the other hand, the computational results can yield precise contour lines corresponding to the computed PEEQ values. Figure 4 suggests that the simulated contour plot is less elongated than the experimental one. The effects of strain hardening exponent and yield strength on PEEQ distribution are not captured clearly by the simulation, as shown in Figure 4, which actually seems to suggest other-

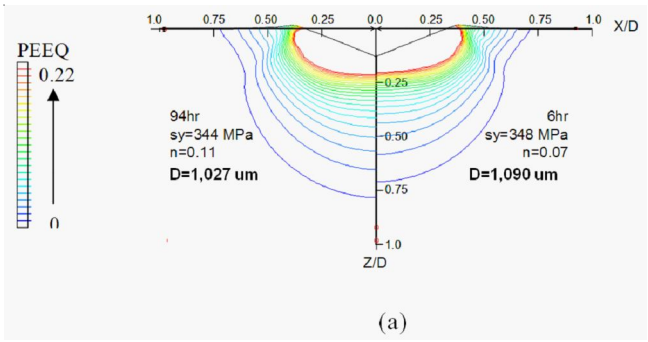

(a)

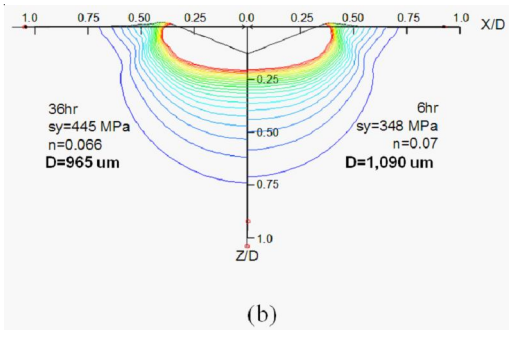

(b)

Figure 4. Simulated contour plot of equivalent plastic strain (PEEQ) distribution underneath Vickers indenter for (a) 6 vs. 94 hrs aged sample (similar σ_y but different n) and (b) 6 vs. 36 hrs aged sample (similar n but different σ_y). Note that the contour line indicates PEEQ=0 from the outermost to PEEQ=0.22 at the innermost.

wise. Note that if the boundary condition for the bottom plane *cde* is changed to no displacement in axis 3, the contour plots in Figure 4 do not change since the vertical distance (sample height) is already a far field condition for the indentation simulation. Furthermore, the main characteristics are the same if the contour plots are taken at the maximum loading, instead of the complete unloading shown in Figure 4.

In order to clearly investigate the effect of strain hardening exponent and yield strength on PEEQ distribution, the 6 hrs aged case, with (σ_y, n) = (348 MPa, 0.07), was used as the reference with three additional cases hypothetically constructed as (σ_y, n) = (348 MPa, 0.3), (175 MPa, 0.07), and (700 MPa, 0.07) for case A, B, and C, respectively. Figures 5(a) shows the effect of the strain hardening exponent; whereas, Figure 5(b) and (c) show the effect of yield strength. It is clear that a higher n tends to make the PEEQ contour plot more elongated with the contour lines curling at the contact surface, due to the large sink-in effect, typically found in the materials with high work hardening behavior (Oliver *et al.*, 1992; Dao *et al.*, 2001). When the material with high work hardening behavior is deformed, the contact region will work harden easily and quickly making the plasticity spread limited in the plane, and the contour line curls to the contact surface. As the deformation continues, the spreading is preferable along the loading direction. For the effect of yield strength shown in Figure 5(b) and (c), the lower yield strength tends to make the PEEQ contour less elongated since the plastic deformation spreads laterally and shallowly. On the other hand, the higher yield strength only affects the plasticity spread in the lateral direction with little in the loading direction. Note that it also shows the *curl-back* contour line at the contact surface similar to the case with high work hardening behavior.

4. Conclusions

Three-dimensional computation modeling of instrumented sharp indentation using the Vickers indenter tip was conducted in order to investigate the deformation field underneath, motivated by the experimental plastic strain mapping in a previous study. The simulation is a useful tool in probing the sole effect of each plasticity parameter, in this case, strain hardening exponent and yield strength. However, the simulated results conducted thus far do not seem to correlate well with the previous experimental findings, in terms of the strain field shape and size. Hypothetical cases were further simulated to confirm the effects suggested by the model. It was found that a higher strain hardening exponent seems to make the strain field more elongated due to the sink-in indentation effect with the contour lines curling back to the contact surface. For the yield strength, the lower value seems to make the strain field less elongated (shallower); whereas, the higher value seems to only decrease the strain field laterally with the curl-back contour lines at the contact surface.

These subtle differences require further investigations. Possible reasons were the accuracy of the hardness-to-strain conversion experimental technique, the experimental contour line drawing (Koeppel *et al.*, 1999), the remaining residual stress (Eriksson *et al.*, 2003) in the sample prior to micro-hardness mapping and the validity of the constitutive relations used in the simulation.

Acknowledgements

The authors would like to thank Anchalee Manonukul for using the ABAQUS license at MTEC.

References

Bucaille, J.L., Stauss, S., Felder, E. and Michler, J. 2003. Determination of plastic properties of metals by instrumented indentation using different sharp indenters. Acta Materialia. 51, 1663-1678.

Chaudhri, M.M. 1998. Subsurface strain distribution around Vickers hardness indentations in annealed polycrystalline copper. Acta Materialia. 46, 3047-3056.

Chollacoop, N., Dao, M. and Suresh, S. 2003. Depth-sensing instrumented indentation with dual sharp indenters. Acta Materialia. 51, 3713-29.

Dao, M., Chollacoop, N., Van Vliet, K.J., Venkatesh, T.A. and Suresh, S. 2001. Computational modeling of the forward and reverse problems in instrumented sharp indentation. Acta Materialia. 49, 3899-3918.

Doener, M.F. and Nix, W.D. 1986. A method for interpreting the data from depth-sensing indention instruments. Journal of Materials Research. 1, 601.

Eriksson, C.L., Larsson, P.L. and Rowcliffe, D.J. 2003. Strain hardening and residual stress effects in plastic zones around indentations. Materials Science and Engineering A. 340, 193-203.

Gouldstone, A., Chollacoop, N., Dao, M., Li, J., Minor, A.M. and Shen, Y.-L. 2007. Indentation across size scales and disciplines: Recent developments in experimentation and modeling. Acta Materialia. 55, 4015-4039.

Harsono, E., Swaddiwudhipong, S. and Liu, Z.S. 2008. The effect of friction on indentation test results. Modelling and Simulation in Materials Science and Engineering. 16, 65001.

Koeppel, B.J. and Subhash, G. 1999. Characteristics of residual plastic zone under static and dynamic Vickers indentation. Wear. 224, 56-67.

Oliver, W.C. and Pharr, G.M. 1992. An Improved Technique for Determining Hardness and Elastic- Modulus Using Load and Displacement Sensing Indentation Experiments. Journal of Materials Research. 7, 1564-1583.

Srikant, G., Chollacoop, N. and Ramamurty, U. 2006. Plastic strain distribution underneath a Vickers indenter: Role of yield strength and work hardening exponent. Acta Materialia. 54, 5171-5178.

Tabor, D. 1951. Hardness of metals. Oxford: Clarendon Press, England, pp. 1-192.